AIAA JOURNAL
Vol. 44, No. 11, November 2006

Due to a production error the original version of this paper appeared with errors in Eqs. (4) and (5). The corrected equations appear in this version.

Managing Flap Vortices via Separation Control

David Greenblatt*
NASA Langley Research Center, Hampton, Virginia 23681-2199

DOI: 10.2514/1.19664

A pilot study was conducted on a flapped semispan model to investigate the concept and viability of near-wake vortex management by means of boundary layer separation control. Passive control was achieved using a simple fairing and active control was achieved via zero mass-flux blowing slots. Vortex sheet strength, estimated by integrating surface pressures, was used to predict vortex characteristics based on inviscid roll-up relations and vortices trailing the flaps were mapped using a seven-hole probe. Separation control was found to have a marked effect on vortex location, strength, tangential velocity, axial velocity, and size over a wide range of angles of attack and control conditions. In general, the vortex trends were well predicted by the inviscid roll-up relations. Manipulation of the separated flow near the flap edges exerted significant control over either outboard or inboard edge vortices while producing small lift and moment excursions. In summary, separation control has the potential for application to time-independent or time-dependent wake alleviation schemes, where the latter can be deployed to minimize adverse effects on ride-quality and dynamic structural loading.

Nomenclature

A	=	semispan wing area, $s \times c$
AR	=	wing aspect ratio
C_L	=	wing lift coefficient
C_l	=	sectional lift coefficient
C_M	=	wing moment coefficient
C_m	=	sectional moment coefficient
C_p	=	time mean pressure coefficient
C_μ	=	oscillatory flow slot momentum coefficient, $h/c(u_j/U_\infty)^2$
c	=	wing chord length
F^+	=	reduced excitation frequency, $f_e L_f/U_\infty$
f_e	=	separation control excitation frequency
h	=	slot width
L_f	=	flap length, from slot to trailing edge
p	=	pressure
q	=	free-stream dynamic pressure
Re	=	Reynolds number based on chord length
r_1	=	vortex radius corresponding to $V_{\theta,\max}$
r_2	=	vortex radius corresponding the edge of the vortical region
s	=	wing semispan length, $b/2$
s_f	=	flap span, $s/3$
U, V, W	=	mean velocities in directions x, y, z
U_∞	=	free-stream velocity
u_j	=	peak slot velocity
V_x, V_r, V_θ	=	mean wake velocities in directions x, r, θ
x, y, z	=	coordinates measured from model leading edge and root
y'	=	coordinate measured from the tip, $s–y$
y'_0	=	coordinate measured from the outboard flap, $2/3s–y$
$(\bar{y}, \bar{z})$	=	vortex centroid
α	=	angle of attack
α_s	=	static stall angle
Γ	=	wing bound circulation
Γ'	=	vortex strength
γ	=	wing vortex sheet strength, $d\Gamma/dy$
ΔH	=	viscous head-loss
δ	=	flap deflection angle
ω_x	=	streamwise vorticity
$\langle\,\rangle$	=	phase-averaged quantity

Subscripts

i	=	inboard
o	=	outboard
t	=	tip
te	=	trailing edge

Superscripts

*	=	with separation control
^	=	nondimensionalization wrt U_∞, b, c

I. Introduction

A. Background

THE hazard posed by powerful vortices trailing large commercial airliners [1–3] is particularly severe near airports where planes fly in close proximity and where the relatively low flight speeds result in increased vortex strength. Although the vortices are usually transported away by self-induction or by atmospheric currents, this is not always the case and several accidents have been attributed to vortex encounters in recent decades [4]. Under present flight rules, the delays due to separation distances are often larger than those dictated by other factors, and thus add to airport delays and congestion [5]. With ever larger airliners anticipated in the future, the perennial desire to destroy vortices, or cause them to dissipate to some acceptable level, is expected to intensify.

Methods proposed for destroying or dissipating vortices generally fall into two categories, namely "turbulence injection" [6,7] into the vortex core and exploitation of unstable growth mechanisms, such that vortices ultimately interact, pinch off, and degenerate into harmless small-scale turbulence [8,9]. For the latter category, time-invariant and time-dependent methods are proffered. (These are also referred to as passive and active methods, but the present terminology is adopted to avoid confusion with boundary layer separation control methods discussed below.) Time-invariant methods rely on modifying the span loading to establish two or more pairs of opposite-signed counter-rotating vortices and allow naturally arising instabilities to bring about their linking and mutual

Presented as Paper 0061 at the 43rd AIAA Aerospace Sciences Meeting and Exhibit, Reno, NV 2005, 10–13 January 2005; received 27 September 2005; revision received 11 May 2006; accepted for publication 22 May 2006.

*NRC Research Associate, Flow Physics & Control Branch; currently Research Scientist, Technical University of Berlin, 8 Mueller Breslau Street, D-10623 Berlin, Germany; david.greenblatt@pi.tu-berlin.de. Senior Member AIAA.

destruction [10–13]. Time-dependent methods that actively force the breakup of vortices are realized, for example, by differentially deflecting inboard and outboard control surfaces ("sloshing" of the lift distribution) [14,15]. This method was tested in a towing tank [16], where measured amplification rates agreed qualitatively with theoretical predictions. Recently, a similar approach was pursued with a view to exploiting the multiple vortex growth mechanisms created by an airplane on approach with flaps down [4]. Despite their inherent appeal, active methods must address issues such as "ride quality, dynamic-load effects on the structure, and the ability to maintain control authority during operation" [17].

When flaps are deployed [18,19] their edge vortices are typically stronger than the tip vortices and they dominate the ensuing wake structure, particularly during approach for landing [20,21]. A stability analysis of a two-vortex pair [22], revealed short wavelength instabilities with growth rates up to 2 times larger than the Crow instability and transient growth mechanisms can amplify an initial disturbance by a factor of 10 to 15 in one-fifth of the time required for the same growth due to instability at the same wavelength. While airliner flaps deliver the required C_L for landing, they are aerodynamically inefficient due to flow separation [23]. Although separated flow is generally associated with aerodynamic inefficiency, here we view it as a resource that can be harnessed to modify lift [24,25], or bound circulation Γ, and therefore has the potential to modify the vortex sheet strength (or shed vorticity) $\gamma = \mathrm{d}\Gamma/\mathrm{d}y$. Since the vortex sheet on a flapped wing rolls up into multiple distinct vortices, boundary layer separation control emerges as a strong candidate for directly controlling, or managing, the individual vortices. Moreover, local control of separation, for example, over some fraction of the flap span, has the potential for locally modifying γ, thereby exerting control over individual vortices while simultaneously minimizing lift excursions. Presently, however, little is known of the efficacy of separation control in the highly three-dimensional flap-edge region.

Active separation control methods [25], in general, provide greater flexibility than passive methods [24] in that they have greater authority and can control the degree of boundary layer separation. Furthermore, separation and attachment can be controlled dynamically [26]. Therefore, if separation control can be shown to be a feasible means of managing trailing vortices, then dynamic separation and attachment can be further exploited to achieve this in a time-dependent manner. Dynamic separation control can then be employed for directly exciting wake instabilities.

B. Objective and Scope

The concept and viability of vortex management via separation control was investigated by conducting a pilot study involving a semispan wing model. Details of the wing design including flaps, pressure ports, and excitation slots are provided in Sec. II. Empirical span-loading data were used together with inviscid vortex roll-up relations (Secs. III.A and IV) to predict the near-field vortex characteristics. Flow field measurements using a seven-hole probe were performed in the near wake of the wing and the vortex characteristics were compared to the inviscid roll-up predictions (Sec. III.B and IV).

This pilot study presently does not address the intermediate or far-field vortex structure. The primary objective was to assess the use of separation control for generating boundary conditions that are consistent with those believed to be effective for time-invariant and time-dependent vortex alleviation strategies. A secondary objective was to assess authority over the vortex while simultaneously minimizing lift and moment excursions. Dynamic perturbation of the vortices, by means of dynamic separation and attachment control, was considered beyond the scope of this paper, but discussed in [27].

II. Experimental Setup

A. Semispan Model

Experiments were performed on a rectangular planform semispan NACA 0015 model wing of aspect ratio AR = 4 (semispan $s = 609.6$ mm, chord $c = 304.8$ mm) cantilevered off the wall of a low-speed wind tunnel (see Figs. 1 for coordinate systems) at $500,000 \leq Re \leq 1,000,000$. The model has a main element and three simple flaps (inboard, outboard, and tip) of equal span ($s_f = s/3$), with the hingeline at 70% chord. Each flap is independently adjustable through a range of −10 deg (upwards) to 40 deg (downwards) with indexed settings in 10 deg increments, denoted $(\delta_i, \delta_o, \delta_t)$. Flap angles are maintained using brackets between the main element and flaps that are flush with the wing lower surface. The model has a blowing slot at the shoulder of each flap, each with a width of 0.76 mm. (The main element has an additional leading-edge slot with a width of 0.5 mm that was not used in this study.) The model was constructed from aluminum, apart from the slot edges that were constructed from stainless steel in order to maintain a 0.25 mm edge. The wing tip plate was square and set to be flush with the edge of the tip flap.

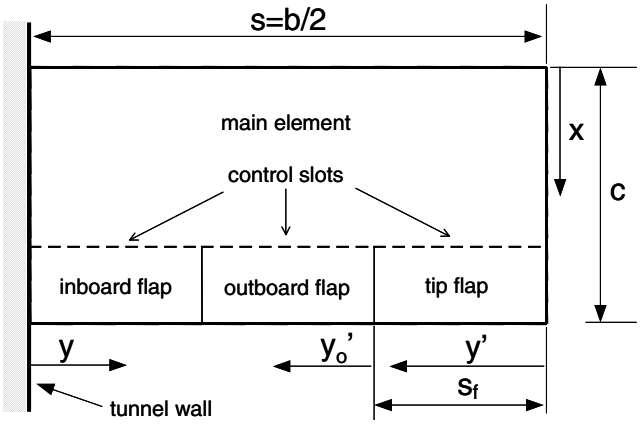

Fig. 1 Plan view schematic of the semispan wing model, showing the layout and coordinate systems.

The maximum turbulence level within the tunnel test section was measured at below 0.1% and the flow uniformity variation without the wing installed was less than 1% across the span and height of the tunnel.

B. Types of Control

The main element is effectively hollow, apart from necessary internal structure, and acts as a plenum for the various slots on the wing surface. It incorporates a main spar that includes three removable internal, sealed partitions and an upper cover plate. Zero mass-flux perturbations are introduced via two voice-coil type actuators that are connected to the subplenums via manifolds. The resulting subplenums are in fluidic communication with an adjacent flap-shoulder slot that produces the perturbations in the reduced frequency range $0.4 \leq F^+ \leq 3$ with $C_\mu \leq 1.5\%$, known to be effective for two-dimensional separation control [25]. The uncertainty in the perturbation amplitude was estimated at $\Delta C_\mu / C_\mu \leq 20\%$. In addition to the active flow control setup described above, passive control was exerted by placing a fairing over the slot between the main element and flap upper surface. This eliminated the small backward facing step introduced by the slot, thereby forming a smooth transition between the main element and flap.

C. Measurement Techniques

The model is further equipped with 165 static pressure ports arranged in a perpendicular spanwise and chordwise grid. The spanwise ports are located at the chordwise locations $x/c = 5/100$, $3/10$, $77/100$, and 1, and are grouped more closely near the tip. The chordwise ports are located at nominal spanwise locations: $y/s = 1/6, 1/2, 5/6$, and $99/100$, and are grouped more closely near the leading edge, while the flaps are equipped with additional ports. Surface pressures were integrated in order to compute aerodynamic coefficients and estimates of pressures within the grid were obtained using a three-dimensional interpolation method. The model is also

equipped with nine dynamic pressure transducers on the wing upper surface. Slot velocities were calibrated using a hot-wire anemometer and actuator performance was monitored using unsteady transducers mounted within the subplenums.

Wing static pressures were measured using a high-speed pressure scanner and unsteady pressures were measured by means of piezoresistive unsteady pressure transducers. The main source of error in the pressure measurements was due to precision, with $C_p \leq \pm 0.02$, based on 95% confidence intervals. A 1.65 mm diameter seven-hole probe was used to make wake measurements at $x/c = 2$, where velocities were calculated by means of a calibration database and a local least-squares interpolation technique. In an independent study [28], the probe was calibrated throughout the entire subsonic regime and an uncertainty analysis was performed using three approaches: 1) an evaluation of the least-squares procedure; 2) an analysis of how pressure measurement uncertainties propagate through the algorithm; and 3) an evaluation of the uncertainty of the algorithm. It was ascertained that flow angles are predicted to within 0.6 deg and velocity is predicted to within 1.0%, both with 99% confidence.

III. Data Reduction Methods

A. Control Predictions Using Inviscid Rollup Relations

Predicting the effect of separation control on flap vortex characteristics was achieved using the method of Betz [29], in the form developed by Donaldson et al. [30] Betz's method does not explicitly treat the roll-up mechanism, but rather employs three conservation relations between the span-loading $\Gamma(y)$ and the rolling-up vortex $\Gamma'(r)$. Betz employed the conservation of vorticity [see Eq. (2) below], and also postulated that the first and second moments of vorticity are conserved [see Eqs. (1) and (3) below]. Despite the relative simplicity of the method, it predicts flap vortex details that are in surprisingly good agreement with aircraft-wake wing tip vortices [30].

Implementation of the method presented a difficulty due to the dearth of theoretical or computational methods capable of accurately predicting the effects of zero-efflux perturbations. To circumvent this problem, empirical data for $\gamma(y) = \Gamma(y)/dy$ were obtained by integrating wing surface pressures (see Sec. II.C). To illustrate the application of the method consider the lift distributions that results from a deflection of the adjacent inboard and outboard flaps, without separation control (baseline case) and with control applied along the length of the flap (controlled case), shown in the top half of Fig. 2. Separation control brings about an approximately uniform increase in lift (or circulation) along the extent of the flap and, consequently a substantial change to $\gamma(y)$ in the vicinity if the flap edge. The lines are third-order polynomial least-squares curves, fitted to data points in the vicinity of the flap edges. The net wing lift increase observed is generally undesirable from the perspective of vortex management (Sec. I.A), but this example is used merely for the purposes of introducing and illustrating the method. Minimization of lift excursions is addressed in Sec. IV.

The lower part of the figure shows the theoretically predicted rolled-up vortices in the so-called Trefftz plane. For relatively complex wing-load distributions, such as that shown in Fig. 2, Donaldson et al. [30] showed that circulation becomes multivalued during the roll-up calculation and thus a single vortex roll-up is not physically possible. They assumed that the vorticity shed between adjacent local $|d\Gamma/dy|$ minima rolls-up into individual vortices [31] and that the local shed vorticity peak between the adjacent minima ($|d\Gamma/dy|_m$), located at $y = y_m$, progresses into the center of the vortex. Using these criteria, the method predicts three distinct vortices in the Trefftz plane (Fig. 2): at the wing tip, A, flap-edge, B, and wing-wall junction, C. These predictions are consistent with observations, at least in the near field considered here ($x/c \leq 2$). The relatively low pressures at the wing tip result from the wing tip vortex being partially rolled up on the upper surface. Without further approximation, this precludes the application of roll-up relations to the tip vortex.

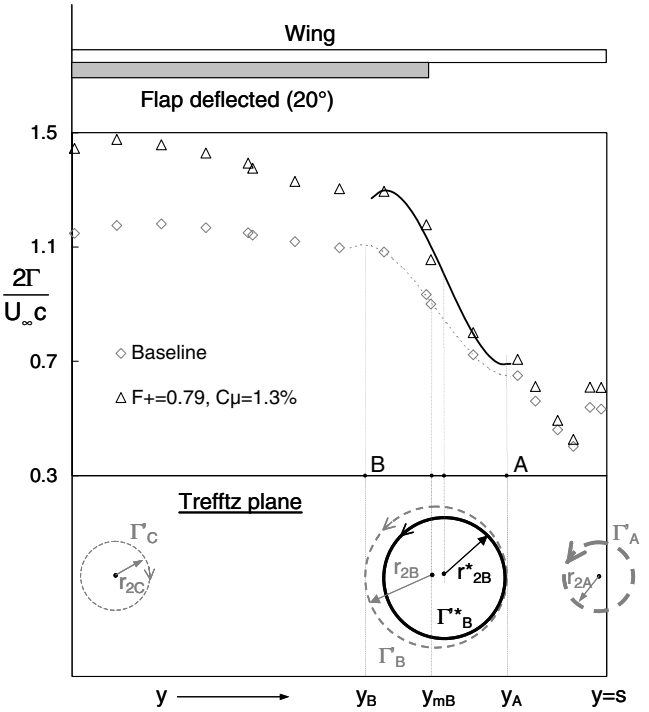

Fig. 2 Schematic illustrating the Donaldson–Betz vortex roll-up method between the span-loading and the Trefftz plane (lower part), using experimental data (upper part), with and without separation control.

Applying the method to the outboard flap vortex (B) for the uncontrolled case, the vorticity between adjacent $|d\Gamma/dy|$ minima y_A and y_B rolls up into a vortex located at the centroid defined by

$$\bar{y}_B \int_{y_B}^{y_A} \frac{d\Gamma(y)}{dy}\, dy = \int_{y_B}^{y_A} y \frac{d\Gamma(y)}{dy}\, dy \tag{1}$$

Using third order polynomials to approximate $\Gamma(y)$ in the flap-edge region, the remaining invariants described above can be written as

$$-\int_{y_B}^{y_A} \frac{d\Gamma(y)}{dy}\, dy = \int_0^{r_{2B}} \frac{d\Gamma'_B(r)}{dr}\, dr \tag{2}$$

and

$$-\int_{y_B}^{y_A} (y - \bar{y}_B)^2 \frac{d\Gamma(y)}{dy}\, dy = \int_0^{r_{2B}} r^2 \frac{d\Gamma'_B(r)}{dr}\, dr \tag{3}$$

Equation (2) is integrated directly to yield the vortex strength

$$\Gamma'_B(r_{2B}) = -\int_{y_B}^{y_A} \frac{d\Gamma}{dy}\, dy = \Gamma(y_B) - \Gamma(y_A) \tag{4}$$

with its centroid, from Eqs. (1) and (4), located at

$$\bar{y}_B = -\frac{1}{\Gamma'_B(r_{2B})} \int_{y_B}^{y_A} y \frac{d\Gamma}{dy}\, dy \tag{5}$$

An expression for the vortex radius that satisfies Eq. (4) (outer core radius) [2], can be derived from Eqs. (2) and (3), and is simply

$$r_{2B} = \frac{y_A - y_B}{2} \tag{6}$$

Finally, using the equation for an inviscid vortex, and a relation similar to that of Eq. (3), the tangential velocity at the center of the vortex is

$$V_{\theta B}(0) = -\frac{1}{\pi} \left(\frac{d\Gamma}{dy} \right)_{y = y_{mB}} \tag{7}$$

The relations expressed in Eqs. (4–7) provide four basic characteristics of the baseline rolled-up vortex. The use of third order polynomials in the flap-edge region (Fig. 2) simplifies the original analysis of [30] and results in algebraic expressions for Eqs. (4–7). An identical procedure to that above is applied to the control case (see Fig. 2).

Simplifying assumptions associated with the above method [32,33], are well known. Nevertheless, when applying the method to a flow control problem, the limitations become less important when comparing changes, for example, between baseline and controlled states: $\Delta\bar{y} = \bar{y}^* - \bar{y}$, $V_\theta^*(0)/V_\theta(0)$, Γ'^*/Γ', and r_2^*/r_2. Furthermore, given the relative simplicity and rapidity of span-loading measurements versus wake-surveys, the method is particularly useful for ascertaining trends.

B. Wake Measurements

All wake measurements were performed in a plane at $x/c = 2$, by means of a seven-hole probe, yielding (U, V, W) as a function of (y, z). Streamwise vorticity was calculated according to

$$\omega_x = \partial W/\partial y - \partial V/\partial z \tag{8}$$

using central differences. Vortex strength in the wake and the vortex centroid were determined by means of the standard definitions:

$$\Gamma_w = \int \omega_x \, dA \tag{9}$$

and

$$(\bar{y}_w, \bar{z}_w) = \frac{1}{\Gamma_w} \int (y, z)\omega_x \, dA \tag{10}$$

where the integration regions were chosen such that $\omega_x \ll \omega_{x,\max}$ at the boundaries.

The tangential velocity (V_θ) and radial coordinate (r) were determined from the in-plane velocity components (V, W) and (y, z) coordinates relative to the vortex centroid, respectively. This allowed direct determination of the peak tangential velocity $V_{\theta,\max}$ and the corresponding inner core radius (r_1), but scatter and asymmetry precluded accurate measurement of r_2. Recall from Sec. III.A, however, that the Donaldson–Betz method predicts a finite centerline peak velocity $V_\theta(0)$, thus $r_1 = 0$.

IV. Discussion of Results

A preliminary assessment of the symmetric wing (no flap deflections) was conducted at $Re = 500,000$ and $Re = 1,000,000$. Surface C_p differences for the two Reynolds numbers were small because the leading-edge slot effectively tripped the boundary layer and the sharp square wing tip fixed separation of the tip flow at the lower wing tip edge. The wing stalled inboard, as expected, at $\alpha = 14$ deg. Pressure measurements on the model, including the region near the wing tip $(y/s > 0.97)$, were consistent with data of other investigations [34,35] that were conducted on models without flaps or slots and at higher Reynolds numbers $(Re \sim 2,000,000)$. It was concluded that the flap slots did not have a noticeable effect on the details of the tip vortex roll-up or span loading. Moreover, the favorable comparison also validated the pressure interpolation scheme mentioned in Sec. II.C.

A. Inboard and Outboard Flap Deflection

The first configuration considered here was the deflection of adjacent inboard and outboard flaps $(\delta_i, \delta_o, \delta_t) = (20, 20, 0$ deg), discussed in Sec. III.A, where zero mass-flux excitation was introduced along the length of the flapped section. Lift coefficient data presented in Figs. 3a and 3b are for the baseline case as well as control applied at two amplitudes, at an inboard location $(y/s = 1/6)$ and for the wing, respectively. As expected, the effect of control inboard (Fig. 3a), where three-dimensional effects are negligible, is similar to that observed on airfoils [25]. At relatively low amplitude

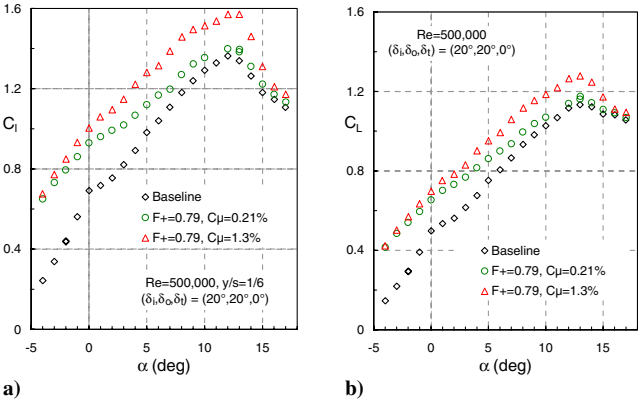

Fig. 3 a) Inboard lift coefficient and b) wing lift coefficient for two forcing amplitudes with inboard and outboard flaps deflected.

$(C_\mu = 0.21\%)$, control is effective at $\alpha < 0$ deg but its effectiveness gradually diminishes as α approaches stall $(\alpha_s \approx 12$ deg). The overall effect of separation control on C_L at both amplitudes is qualitatively similar to that inboard, but the differences between baseline and control are smaller. This is because separation control is only effective over the flapped fraction of the span, whereas lift over the remainder of the span toward the tip is not significantly affected (e.g., Fig. 2). Nevertheless, separation control is effective across the entire flap span and trailing-edge pressure recovery ($C_{p,\text{te}}$; not shown) shows a nearly uniform change across the flap span.

Detailed solid and wake blockage effects can be taken into account using the methods described in [34]. However, the applied correction is similar in both the baseline and controlled cases. Thus, for the present data, such corrections were not performed because the primary interest here was the changes to the span loading.

The experimentally determined span loading (e.g., Fig. 2) was used as input to the roll-up relations [Eqs. (1–7)], to predict the effect of separation control on the four basic characteristics of the flap vortex for the baseline and two control cases discussed above. The data are shown in dimensionless form as a function of α [Figs. 4a–4d]. In general, the predictions indicate that separation control

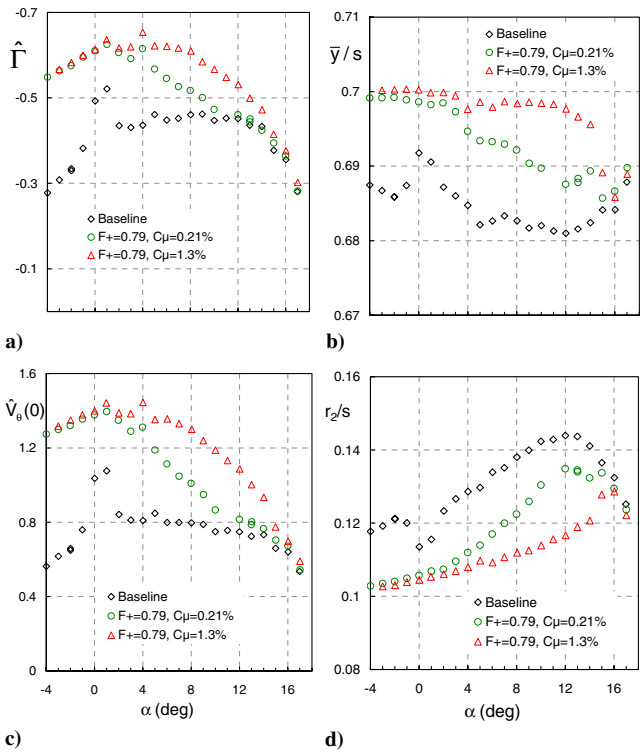

Fig. 4 Donaldson–Betz predictions of controlled vortex characteristics in dimensionless form: a) strength; b) centroid; c) peak velocity; and d) outer core radius, using experimentally determined span loading.

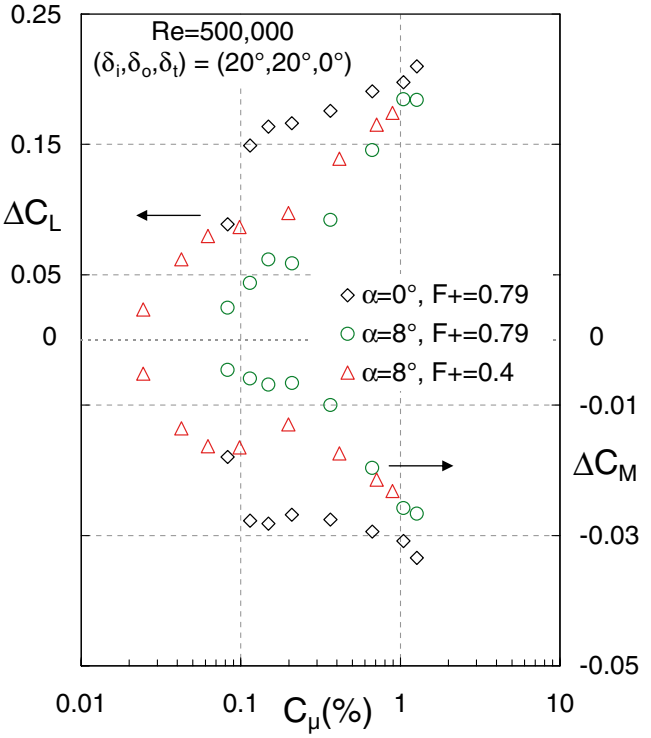

Fig. 5 Changes to lift and moment coefficient as a function of forcing amplitude at two angles of attack and two forcing frequencies.

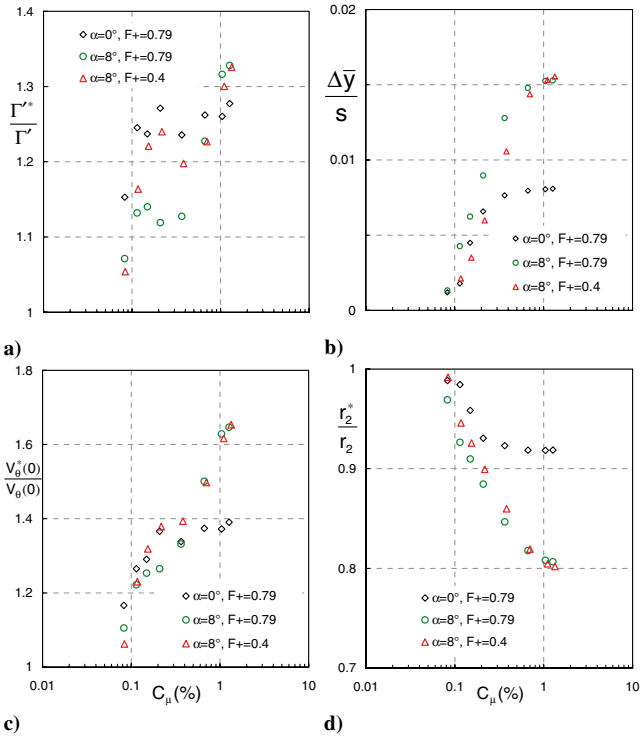

Fig. 6 Donaldson–Betz predictions of vortex characteristics as a function of forcing amplitude corresponding to the data in Fig. 5.

strengthens the vortex [Fig. 4a], moves the centroid outboard [Fig. 4b], increases the peak velocity [Fig. 4c] and reduces the vortex size [Fig. 4d]. The extent to which vortex strength and peak velocity are controlled depends to some extent on the degree of separation control. At low α significant authority is achieved, but control over vortex strength and peak velocity diminishes as the wing approaches stall ($\alpha_s \approx 12$ deg). Nevertheless, meaningful authority is exerted over the centroid location and vortex size for a wide range of α up to stall. This is true for both low and high amplitude control, even when the effect on wing lift is small.

Control of an initially separated flow affects the aerodynamic coefficient in different ways, depending on the angle of attack (or flap deflection). At low angles of attack, the flow is seen to fully attach when some threshold perturbation level (C_μ) is exceeded. At higher angles of attack, a coefficient such as C_L varies gradually, approximately logarithmically, with C_μ. These effects are illustrated with respect to relatively low and high angles ($\alpha = 0$ and 8 deg), where two different forcing frequencies are employed at the higher angle for illustrative purposes (Fig. 5). At $\alpha = 0$ deg, relatively large changes in the aerodynamic coefficients are evident at $C_\mu \approx 0.15\%$ and increasing the forcing amplitude thereafter has little effect. These effects are reflected to some degree in the control authority over the basic vortex characteristics [Figs. 6b–6d] where changes are relatively small and authority saturates at a relatively low forcing level. At $\alpha = 8$ deg the effect on C_L and hence vortex characteristics is more gradual. Also, the thicker separated shear layer represents a larger resource for control and hence the control authority over the vortex is greater. The same would be true at lower angles of attack with greater flap deflections.

B. Segmented Actuation and Zonal Control

Separation control for the purpose of performance improvement is generally applied over the entire span of a separated region, resulting in significant changes to aerodynamic indicators. Thus if separation control was to be deployed in a time-dependent manner, it could potentially result in significant force and moment oscillations. A similar problem exists where control surfaces are used to perturb vortices [15,17,36]. We address this problem in the following manner: if perturbations are applied locally along some fraction or segment of the slot, it is possible that separation control can be achieved over a finite zone of the flap. Then, in principle, the local vortex sheet $\gamma = d\Gamma/dy$ can be varied and hence control can be exerted over a specific vortex, leaving the remainder of the wake unchanged, with considerably smaller excursions in lift and moment. Applying control over different parts of the flap periodically can then, in principle, eliminate load oscillations while facilitating time-dependent control of the vortices by so-called sloshing [15] of the lift distribution. This is similar to the methods that oscillate control surfaces [4,15], but with two important differences: 1) the flap is maintained at a fixed deflection, and 2) control on a single flap is sufficient to perturb the vortex with minimal load variations. Dynamic aspects of this approach are discussed in [27].

Because of the dearth of separation control data available in a three-dimensional environment, applied over a fraction of the span, we digress slightly here to discuss some details. Consider the application of separation control over the inboard and outboard halves of the slot, where trailing-edge pressures ($C_{P,\text{te}}$) corresponding to these two cases are shown in Figs. 7a and 7b, respectively. $C_{P,\text{te}}$ indicates the degree of pressure recovery and hence "control effectiveness." For these data, segmented actuation

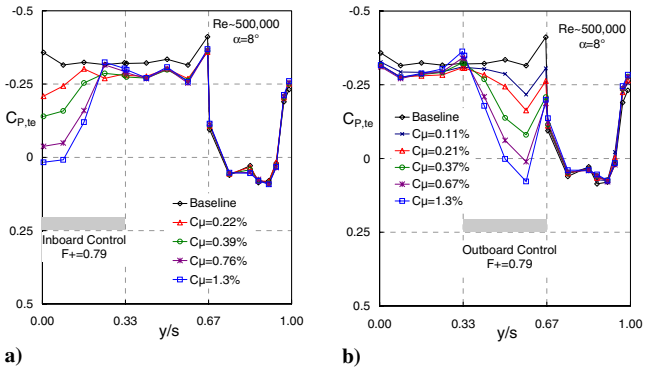

Fig. 7 Spanwise flap trailing-edge pressure recovery for a) inboard separation control and b) outboard separation control for the $(\delta_i, \delta_o, \delta_t) = (20, 20, 0$ deg) configuration.

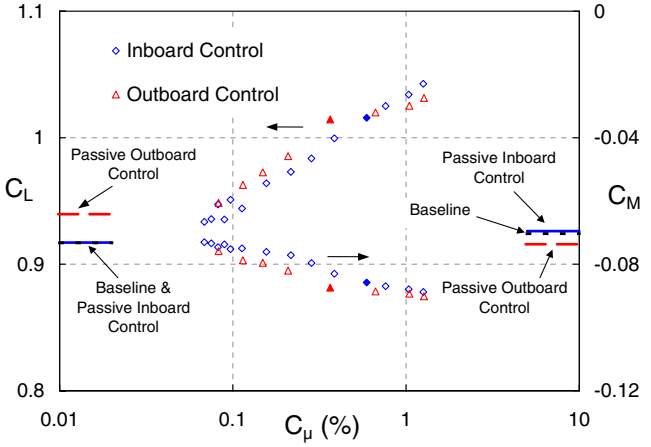

Fig. 8 Effect of passive and active, inboard and outboard, separation control on overall wing lift and moment coefficients.

was achieved using the fairing (described in Sec. II) to seal the part of the slot not being used. The net result is that active separation control applied on one half of the flap is accompanied by mild passive control on the other half. Control effectiveness clearly increases with increasing C_μ and this can also be seen with respect to the effect on wings C_L and C_M (Fig. 8). Nevertheless, the changes in C_L and C_M are smaller than when the separation is controlled over the entire flap (cf. Fig. 5). A comparison of Figs. 7a and 7b shows that outboard control is more efficient in attaching the flow, in the sense that smaller C_μ is required for a given pressure recovery. Outboard control is also more effective in that the extent over which the pressure recovers is larger even at smaller C_μ. This is also true for passive control, where small changes in the aerodynamic coefficients occur ($\Delta C_L = 0.02$, $\Delta C_M = 0.003$) with outboard passive control, whereas no effect is evident with inboard passive control.

The reason for these differences must somehow be related to the different three-dimensional environment of the two control scenarios. It is suggested here that outboard control is more efficient and effective because the flap-edge vortex aids in the transfer of high-momentum fluid to the surface from below the wing. Hence outboard separation control is the result of a combination of spanwise vortices produced by excitation of the free shear layer superimposed approximately orthogonally on the flap-edge vortex. In contrast, inboard control terminates at the wind tunnel wall-wing junction, where a horseshoe vortex forms [37], and no fluid can be drawn from the lower part of the wing. It is not clear whether the junction vortex increases or decreases separation control effectiveness.

The difference in span loading for inboard and outboard control is shown for the passive case [Fig. 9a] and an active case [Fig. 9b]. The active case was selected such that both inboard and outboard control produce similar C_L and C_M (see filled symbols in Fig. 8). The roll-up relations predict a relatively small effect of passive control with the exception of the vortex centroid and size [Figs. 10a–10d]. This is due

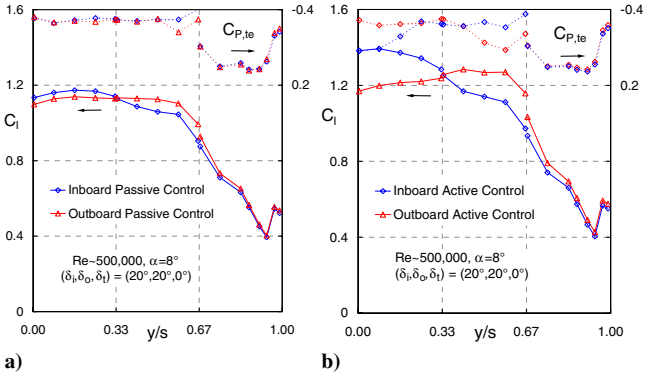

a) b)

Fig. 9 Span-loading for a) passive and b) active inboard and outboard control.

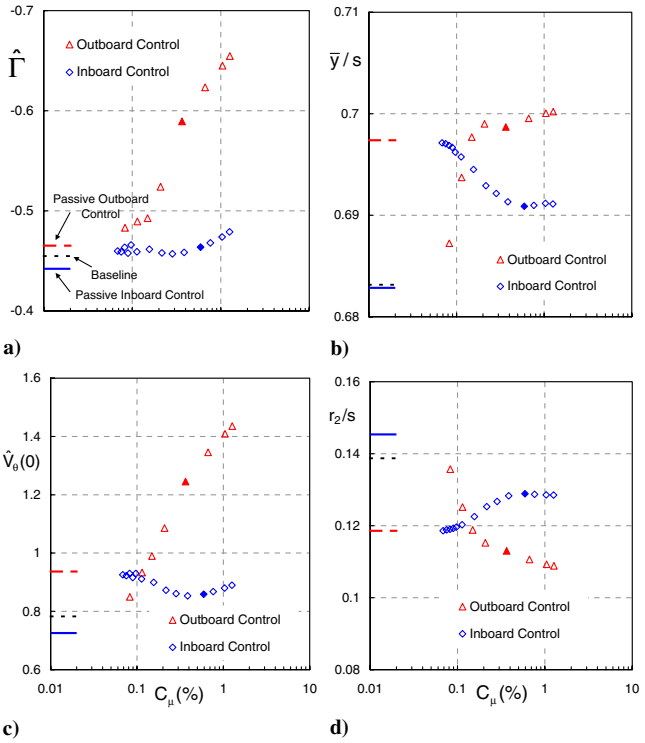

a) b) c) d)

Fig. 10 Dimensionless vortex characteristics predicted using the Donaldson–Betz roll-up relations, corresponding to the wing lift and moment coefficients shown in Fig. 8.

to the relatively large influence on C_l in the vicinity of the flap-edge exerted by the passive device [Fig. 9a], despite the small overall change in lift (see Fig. 8). Active outboard control exerts substantial authority over the all of the vortex characteristics because the vortex sheet is significantly altered in the region where the vortex rolls up [e.g., Fig. 9b]. Changes generally have a logarithmic dependence on C_μ, with the exception of the vortex centroid and size, where authority saturates at $C_\mu \approx 0.15$. Small changes occur with the application of inboard control because alterations to the vortex sheet occur remotely from flap-edge vortex. The filled symbols in the figures correspond to cases of similar C_L and C_M (see Fig. 8) and thus indicate the degree of control that can be exerted by oscillating between the two states in a quasisteady manner. Note that data corresponding to inboard active control are shifted due to the effect of the passive outboard fairing that was employed to seal the outboard part of the slot. The advantage of the active method over the passive one is clearly illustrated here. In principle, active control from different locations can be used to produce precisely the same lift and can exert substantial and varied control over the vortices. Passive methods, on the other hand, operate in a simple on–off manner, thus limiting control flexibility over lift and vortex characteristics.

Seven-hole probe measurements at $x/c = 2$ for passive and active control, corresponding to the span loadings illustrated in Figs. 9a and 9b (filled symbols in Figs. 8 and 10), are shown in Figs. 11a–11d (vorticity and in-plane velocity) and 12a–12d (streamwise velocity). Changes to the vortex characteristics between inboard and outboard control, both passive and active, are compared with those calculated from the roll-up relations in Table 1. In general, the predictions of centroid movement and peak velocity ratio are good, whereas vortex strength and size ratio only show the correct trends. Both roll-up relations and wake measurements show the surprising result that passive control has a larger effect on the vortex centroid. This serves to emphasize the fact that controlling the vortex sheet strength in the vicinity of the flap edge can have a large effect on the centroid without significant changes to the overall aerodynamic loads. The comparison in Table 1 also serves to illustrate the limitations of the roll-up method. For example, simple passive control increases the vortex strength by 23% where this is not evident from the 5%

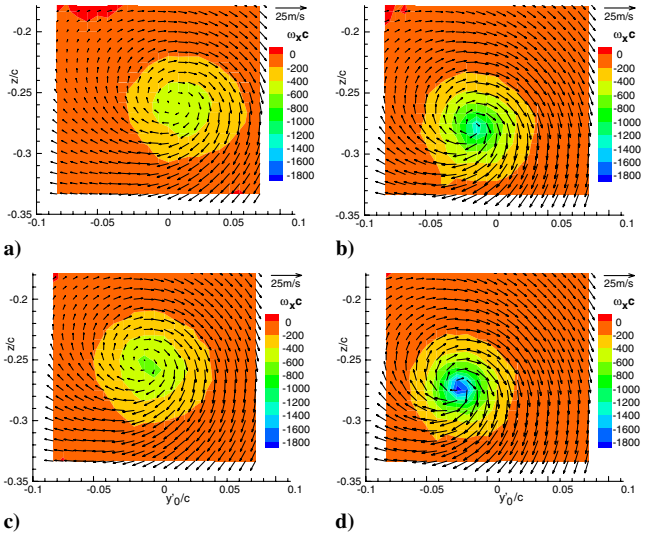

Fig. 11 Seven-hole probe measurements of axial vorticity and in-plane velocity for the scenarios: a) passive inboard control; b) passive outboard control; c) active inboard control; d) active outboard control ($x/c = 2$).

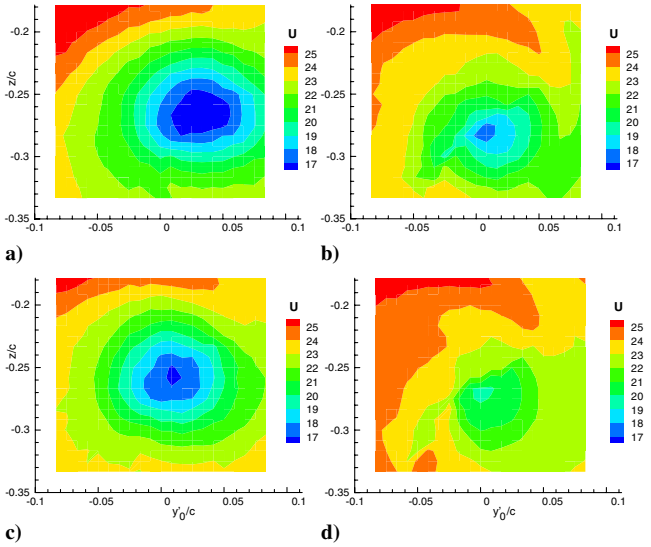

Fig. 12 Seven-hole probe measurements of axial velocity for the scenarios: a) passive inboard control; b) passive outboard control; c) active inboard control; d) active outboard control ($x/c = 2$).

increase predicted from the span loading. The main reason for the poorer predictions is that the method neglects viscous effects which become more important when dealing with the roll-up of separated shear layers.

For different wings, the rate of trailing vortex roll up exhibits large variations depending on aspect ratio and planform (or load distribution). An investigation similar to this one but with larger wing aspect ratios [34], showed only minor changes to the vortex between $x/c = 2$ and 5. On this geometry and that of [34] the vortex is extensively rolled up around the tip of the wing before it is even shed into the wake. Therefore it can be expected that the vortices are almost fully formed by $x/c = 2$. A similar argument can be applied to the inboard flaps where an even smaller fraction of the vortex sheet rolls in to the vortex.

However, without measurements further downstream it cannot be stated conclusively that the near-wake effects will persist into the intermediate and far wake. Nevertheless, based on the present surface pressure data, there can be little argument that separation control fundamentally alters the vortex sheet. And data from a variety of aircraft showed that modification of the vortex sheet directly correlates with far vortex field data, particularly with regard to centroid predictions [30].

As a general rule it was assumed that the presence of the probe had a similar effect on the vortex structures in both controlled and uncontrolled cases. Thus the errors associated with the differences and ratios in vortex properties were assumed to be negligibly small due to the already small errors associated with the absolute velocity measurements (see Sec. II.C).

Separation control also brings about changes to the vortex axial velocity, on the order of $0.25U_\infty$ [Figs. 12a–12d]. This can be explained qualitatively using Batchelor's [38] analysis applied here to the flap vortex by considering a streamline that extends from upstream of the wing through the vortex centerline (also see [39]).

Table 1 Comparison of vortex changes based on inviscid roll-up relation predictions and near-wake measurements

	Partial flap-passive control		Partial flap-active control	
	7-hole probe	Donaldson–Betz Method	7-hole probe	Donaldson–Betz Method
$\Delta\bar{y}/s$ (%)	1.3	1.5	0.82	0.78
Γ'^*/Γ'	1.23	1.05	1.17	1.27
$V^*_{\theta,\max}/V_{\theta,\max}$	1.30	1.29	1.38	1.45
r_1^*/r_1	0.71	——	0.62	——
r_2^*/r_2	——	0.82	——	0.88

The axial velocity on the centerline can then be written as

$$\frac{V_x(0)}{U_\infty} = \sqrt{1 + \frac{[p_\infty - p(0)] - \rho g \Delta H}{\rho U_\infty^2/2}} \tag{11}$$

where the fist term in the quotient on the right hand side is the pressure drop in the vortex [$\propto (\Gamma/r_1)^2$] [39] and the second term is a head-loss representing viscous losses. Considering the increased circulation and decreased size associated with the controlled vortex (Table 1), it is clear from Eq. (11) that separation control acts to increase the vortex centerline axial velocity. In addition, viscous losses in an attached boundary layer will be significantly less than those in a thicker separated shear layer. Thus control acts to further increase the centerline velocity by reducing the viscous head-loss. It is therefore a combination of increased pressure drop and decreased head-loss that are jointly responsible for the higher axial velocities.

The roll-up relations assume a flat vortex sheet and roll-up and thus do not account for vertical centroid displacements. The overall displacements measured in the wake are shown in the (y, z) map in Fig. 13 and indicate that control also exerts an effect in the vertical z direction. The passive and active control centroids represent data at similar C_L, whereas the "no control" and "full flap control" cases correspond to $\Delta C_L = 0.17$. Recall that active-inboard control is accompanied by passive outboard control, and vice versa, due to the

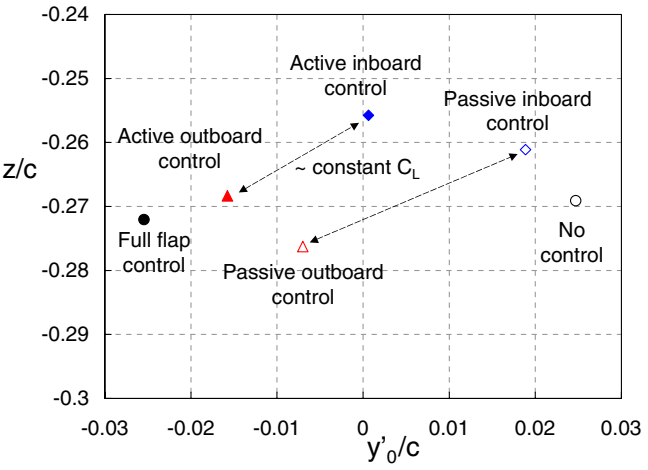

Fig. 13 Vortex centroid map in the (y, z) plane, illustrating the two-dimensional vortex excursions resulting from separation control ($x/c = 2$).

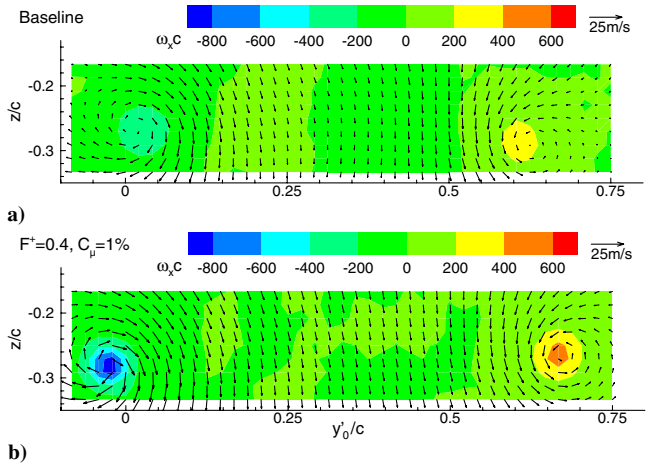

Fig. 14 Seven-hole probe measurements of axial vorticity at $\alpha = 8$ deg for a) baseline and b) control cases in the wake of the outboard flap ($x/c = 2$).

deployment of the fairing. The maps show that different mode shapes could conceivably be excited by time-dependent separation control, but in general this would introduce variation in overall lift. In principle, this could be overcome on a configuration that employs control on more than one flap, where different mode shapes could be excited using control on one flap while overall lift is maintained constant by control on a second flap.

C. Outboard Flap Deflection

1. *Full-Span Flap Control*

The second flap configuration considered was the deflection of the outboard flap alone: $(\delta_i, \delta_o, \delta_t) = (0, 20, 0$ deg). This resulted in a substantial counter-rotating inboard vortex in addition to the outboard vortex considered previously. Management of the counter-rotating inboard vortex is considered important due to its prevalence in many vortex alleviation strategies [10,13]. With control applied along the span of the flap, wing aerodynamic coefficient excursions were qualitatively similar to those for the previous case but 50% smaller, consistent with the shorter flap span. Nevertheless, control exerted considerable authority over γ at the flap edges and low amplitude excitation (C_μ) was effective to higher angles of attack. Corresponding wake measurements are shown in Figs. 14a, 14b, 15a, and 15b, with control at $C_\mu = 1\%$, and are compared with the roll-up predictions in Table 2. In general, the changes to the outboard vortex characteristics are of the same order as those for the combined inboard and outboard flap deflections (c.f. Sec. IV.B and Table 1),

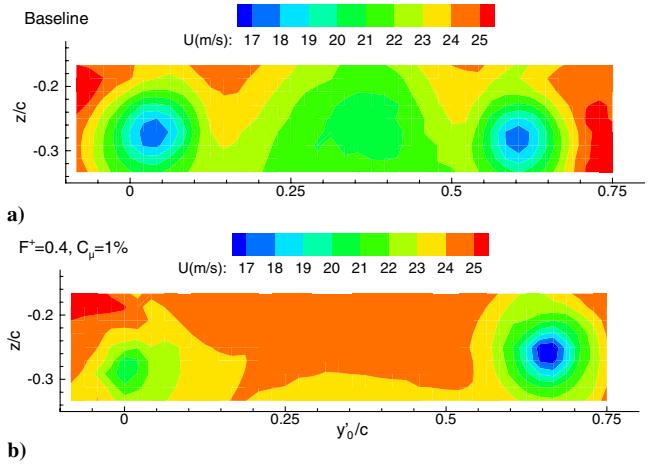

Fig. 15 Seven-hole probe measurements of axial velocity at $\alpha = 8$ deg for a) baseline and b) control cases in the wake of the outboard flap ($x/c = 2$).

Table 2 Effect of separation control on the outboard flap trailing vortices

	Outboard vortex		Inboard vortex	
	7-hole probe	Donaldson–Betz Method	7-hole probe	Donaldson–Betz Method
$\Delta\bar{y}/s$ (%)	−2.32	−2.07	2.62	0.93
Γ^*/Γ'	1.36	1.35	1.35	1.76
$V^*_{\theta,\max}/V_{\theta,\max}$	1.44	1.82	1.08	1.97
r^*_1/r_1	0.49	——	0.57	——
r^*_2/r_2	——	0.74	——	0.90

although greater authority is exerted over the vortex centroid and size. The reasonable prediction of the outboard vortex centroid is evidence that the inboard edge of the flap does not significantly affect the near-field roll-up of the outboard flap. Rather, it is the local changes in γ that dominate. It is encouraging to note that authority over the vortex is maintained despite the shorter flap and corresponding 50% smaller lift excursions.

Changes to both inboard and outboard vortex strength, measured in the wake, are similar when each is referenced to its baseline value and thus the relative strength of the vortices remains constant for baseline and control. A comparison with the roll-up relations shows that the inboard vortex trends are not as well predicted. This may be a further limitation of the roll-up method, which historically was never validated for counter-rotating vortices [40]. An additional anomaly associated with the inboard vortex is that the axial velocity decreases with the application of control. This is contrary to that observed for the outboard vortex and also contradicts conventional arguments, such as that presented in Sec. IV.B.

2. *Segmented Actuation*

In an attempt to maintain vortex control authority while further minimizing lift and moment excursions, perturbations were introduced from inboard and outboard halves of the flap, respectively. As expected, control for both of these cases resulted in relatively small overall changes to the aerodynamic indicators, for example, for both outboard and inboard control: $\Delta C_L \leq 0.05$ and $\Delta C_M \leq 0.01$ over the full range of control amplitude (see Fig. 16). Despite these small changes, separation is controlled locally, as can be seen by the pressure recoveries associated with both inboard and outboard perturbations and the associated different span loadings (e.g., Fig. 17). Controlling separation near the edge of a single flap in this manner, corresponding to a relatively small fraction of the semispan ($y/s = 1/6$ presently), clearly has advantages from a wake management point of view. This is because localized separation control produces small overall changes to the wing C_L but introduces a relatively large modification to the vortex sheet peak and hence the vortex centroid.

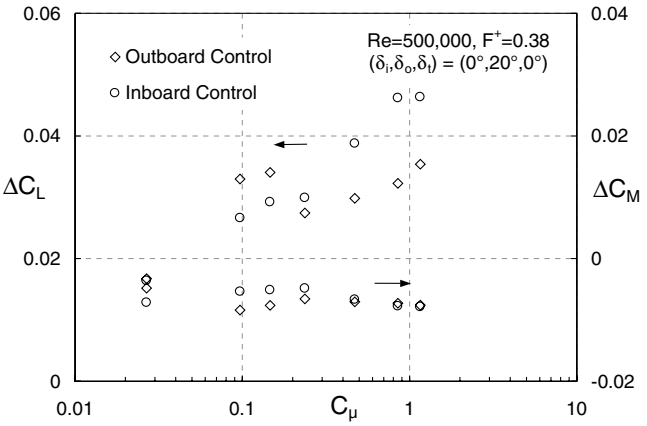

Fig. 16 Lift and moment coefficients corresponding to perturbations introduced on the inboard and outboard halves of the outboard flap at $\alpha = 8$ deg.

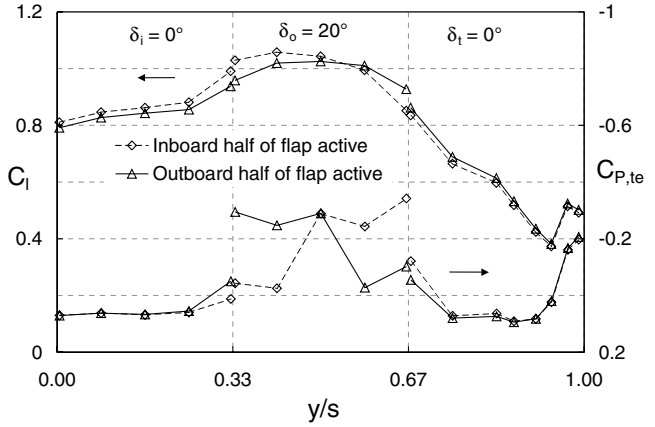

Fig. 17 Span-loading and trailing-edge pressure recovery for control introduced on the inboard and outboard halves of the outboard flap at $\alpha = 8$ deg.

Wake measurements were performed (not shown) and an overall comparison of the vortex characteristics are shown in Tables 3 and 4. It is evident that the application of control in the vicinity of the flap edges does not diminish authority over either the outboard vortex (Table 3) or the inboard vortex (Table 4). Also the relative strengths of the vortices can be significantly varied with small changes to the aerodynamic loads. For example, the ratio of inboard to outboard vortex strength is varied from 0.55 (outboard control) to 0.87 (inboard control) with $\Delta C_L \approx 0.01$. Note that even with inboard control, the outboard vortex is stronger, although the peak inboard vorticity is more than double the outboard peak in this instance (not shown). As in the case of full flap-span control, the roll-up predictions are inferior for the inboard vortex.

V. Concluding Remarks

The concept and viability of managing vortices trailing wing flaps by means of active and passive separation control, was demonstrated experimentally. Separation control was found to have a marked effect on vortex location, strength, tangential velocity, axial velocity, and size over a wide range of flap deflections, angles of attack, and control conditions. In many instances the quantitative vortex characteristics were well predicted by the inviscid roll-up relations.

Table 3 Effect of segmented separation control on the outboard vortex trailing the outboard flap

	Inboard control		Outboard control	
	7-hole probe	Donaldson–Betz Method	7-hole probe	Donaldson–Betz Method
$\Delta\bar{y}/s$ (%)	−0.34	−0.48	−2.50	−2.21
Γ'^*/Γ'	1.03	1.09	1.24	1.05
$V^*_{\theta,\max}/V_{\theta,\max}$	0.94	1.17	1.54	1.36
r_1^*/r_1	0.89	——	0.44	——
r_2^*/r_2	——	0.93	——	0.77

Table 4 Effect of segmented separation control on the inboard vortex trailing the outboard flap

	Inboard control		Outboard control	
	7-hole probe	Donaldson–Betz Method	7-hole probe	Donaldson–Betz Method
$\Delta\bar{y}/s$ (%)	2.73	1.38	0.09	−0.38
Γ'^*/Γ'	1.32	1.38	1.01	1.19
$V^*_{\theta,\max}/V_{\theta,\max}$	1.25	1.61	0.85	1.18
r_1^*/r_1	0.41	——	0.91	——
r_2^*/r_2	——	0.86	——	1.01

Separation control applied near the flap edges exerted significant control over either outboard or inboard edge vortices while producing relatively small lift and moment excursions. The method is now in a position to be tested in a wind tunnel with a longer test section, a tow tank, or even on an aircraft.

It is believed that this method will have significant appeal from an industry perspective due to its retrofit potential with no impact on cruise (separation control devices are tucked away in the cove); low operating power requirements (separated flow instabilities are exploited); small lift oscillations when deployed near flap edges; and significant flexibility (application to different high-lift systems or different flight conditions). The large disparity between the scales characterizing dynamic separation control (fraction of flap chord) and those characterizing wake instabilities (multiple of wingspan), can facilitate perturbation of the vortices from arbitrarily long wavelengths down to wavelengths less than a typical wingspan.

Acknowledgments

This work was performed while the author held a National Research Council–NASA Langley Research Center Associateship. The author wishes to thank W. L. Sellers III, A. E. Washburn, M. J. Walsh, L. P. Melton, L. N. Jenkins, D. H. Neuhart, J. C. Lin, G. S. Jones, S. A. Gorton, G. C. Greene, M. R. Khorrami, I. J. Wygnanski (University of Arizona), and H. M. Nagib (IIT, Chicago) for their active assistance and many fruitful discussions. The author also wishes to thank R. D. White, A. Barnes, and R. L. Clark for their exceptional technical support.

References

[1] Green, S. I., "Wing Tip Vortices," in *Fluid Vortices*, edited by S. I. Green, Kluwer Academic Press, Dordrecht, The Netherlands, 1995, Chap. 1, pp. 1–33.

[2] Spalart, P. R., "Airplane Trailing Vortices," *Annual Review of Fluid Mechanics*, Vol. 30, 1998, pp. 107–138.

[3] Rossow, V. J., "Lift-Generated Vortex Wakes of Subsonic Transport Aircraft," *Progress in Aerospace Sciences*, Vol. 35, No. 6, 1999, pp. 507–660.

[4] Crouch, J. D., Miller, G. D., and Spalart, P. R. "Active-Control System for Breakup of Airplane Trailing Vortices," *AIAA Journal*, Vol. 39, No. 12, 2001, pp. 2374–2381.

[5] Robinson, J. J., "A Simulation-Based Study of the Impact of Aircraft Wake Turbulence Weight Categories on Airport Capacity," AGARD CP-584, 1996, pp. 22-1–22-15.

[6] Dunham, R. E., Jr., "Unsuccessful Concepts for Aircraft Wake Vortex Minimization," NASA SP-409, 1977, pp. 221–250.

[7] Rossow, V. J., "Prospects for Alleviation of Hazard Posed by Lift-Generated Wakes," DOT/FAA/SD-92/1.1, 1991, pp. 22-1–22-40.

[8] Scorer, R. S., "Natural Aerodynamics," Pergamon, New York, 1958.

[9] Crow, S. C., "Stability Theory for a Pair of Vortices," *AIAA Journal*, Vol. 8, No. 12, 1970, pp. 2172–2179.

[10] Rennich, S. C., and Lele, S. K., "Method for Accelerating the Destruction of Aircraft Wake Vortices," *Journal of Aircraft*, Vol. 36, No. 2, 1999, pp. 398–404.

[11] Rossow, V. J., "Theoretical Study of Lift-Generated Vortex Wakes Designed to Avoid Rollup," *AIAA Journal*, Vol. 13, No. 4, 1975, pp. 476–484.

[12] Cliffone, D. L., and Orloff, K. L., "Far Field Wake-Vortex Characteristics of Wings," *Journal of Aircraft*, Vol. 12, No. 5, 1975, pp. 464–470.

[13] Ortega, J. M., Bristol, R. L., and Savas, Ö., "Experimental Study of the Instability of Unequal-Strength Counter-Rotating Vortex Pairs," *Journal of Fluid Mechanics*, Vol. 474, 2003, pp. 35–84.

[14] Crow, S. C., "Panel Discussion," in *Aircraft Wake Turbulence and Its Detection*, edited by J. H. Olsen, A., Goldburg, and M. Rogers, Plenum Press, New York, 1971, pp. 580–582.

[15] Crow, S. C., and Bate, E. R., "Lifespan of Trailing Vortices in a Turbulent Atmosphere," *Journal of Aircraft*, Vol. 13, No. 7, 1976, pp. 476–82.

[16] Bilanin, A. J., and Widnall, S. E., "Aircraft Wake Dissipation by Sinusoidal Instability and Vortex Breakdown," AIAA Paper 73-107, 1973.

[17] Crouch, J. D., "Forcing the Breakup of Airplane Trailing Vortices," *Conference on Capacity and Wake Vortices, Imperial College of*

Science, Technology and Medicine, London, England, Report No. AD-A397491, 2001.
[18] Rudolph, P. K. C., "High-Lift Systems on Commercial Subsonic Airliners," NASA CR 4746, 1996.
[19] van Dam, C. P., "The Aerodynamic Design of Multi-Element High-Lift Systems for Transport Airplanes," *Progress in Aerospace Sciences*, Vol. 38, No. 2, 2002, pp. 101–144.
[20] de Bruin, A. C., Hegen, S. H., Rohne, P. B., and Spalart, P. R., "Flow Field Survey in the Trailing Vortex System Behind a Civil Aircraft Model at High Lift," AGARD CP-584, 1996, pp. 25.1–25.12.
[21] Bellastrada, C., Breitsamter, C., and Laschka, B., "Investigation of Turbulent Wake Vortex Originating From a Large Transport Aircraft in Landing Configuration," *Proceedings of the Confederation of European Aerospace Societies Aerospace Aerodynamics Research Conference*, 2002, pp. 31.1–31.10.
[22] Crouch, J. D., "Instability and Transient Growth for Two Trailing-Vortex Pairs," *Journal of Fluid Mechanics*, Vol. 350, 1997, pp. 311–330.
[23] Rumsey, C. L., and Ying, S. X., "Prediction of High Lift: Review of Present CFD Capability," *Progress in Aerospace Sciences*, Vol. 38, No. 2, 2002, pp. 145–180.
[24] Lin, J. C., "Review of Research on Low-Profile Vortex Generators to Control Boundary-Layer Separation," *Progress in Aerospace Sciences*, Vol. 38, No. 4, 2002, pp. 389–420.
[25] Greenblatt, D., and Wygnanski, I., "Control of Separation by Periodic Excitation," *Progress in Aerospace Sciences*, Vol. 37, No. 7, 2000, pp. 487–545.
[26] Greenblatt, D., Nishri, B., Darabi, A., and Wygnanski, I., "Dynamic Stall Control by Periodic Excitation. Part 2: Mechanisms," *Journal of Aircraft*, Vol. 38, No. 3, 2001, pp. 439–447.
[27] Greenblatt, D., Melton, L., Yao, C., and Harris, J., "Active Control of a Wing Tip Vortex," *Proceedings of the 23rd AIAA Applied Aerodynamics Conference*, AIAA Paper 2005-4851, 2005.
[28] Johansen, E. S., Rediniotis, O. K., and Jones, G., "The Compressible Calibration of Miniature Multi-Hole Probes," *Journal of Fluids Engineering*, Vol. 123, No. 1, March 2001, pp. 128–138.
[29] Betz, A., "Behavior of Vortex Systems," *Zeitschrift fur Angewandte Mathematik und Mechanik*, Vol. 12, No. 3, June 1932; see NACA TM 713, June 1933.
[30] Donaldson, C duP., Snedeker, R. S., and Sullivan, R. D., "Calculation of Aircraft Wake Velocity Profiles and Comparison with Experimental Measurements," *Journal of Aircraft*, Vol. 11, No. 9, 1974, pp. 547–555.
[31] Yates, J. E., "Calculation of Initial Vortex Roll-Up in Aircraft Wakes," *Journal of Aircraft*, Vol. 11, No. 7, 1974, pp. 397–400.
[32] Moore, D. W., and Saffman, P. G., "Axial Flow in Laminar Trailing Vortices," *Proceedings of the Royal Society of London A*,Vol. 333, No. 1595, 1973, pp. 491–508.
[33] Widnall, S. E., "The Structure and Dynamics of Vortex Filaments," *Annual Review of Fluid Mechanics*, Vol. 7, 1975, pp. 141–165.
[34] McAlister, K. W., and Takahashi, R. K. "NASA 0015 Wing Pressure and Trailing Vortex Measurements" NASA TP 3151 (AVSCOM Technical Report 91-A-003), November 1991.
[35] Spivey, W. A., and Morehouse, G. G., "New Insights into the Design of Swept-Tip Rotor Blades," *26th National Annual Forum Proceedings of the American Helicopter Society*, 1970.
[36] Chevalier, H., "Flight Test Studies of the Formation and Dissipation of Trailing Vortices," *Journal of Aircraft*, Vol. 10, No. 1, 1973, pp. 14–18.
[37] Simpson, R. L., "Junction Flows," *Annual Review of Fluid Mechanics*, Vol. 33, 2001, pp. 415–443.
[38] Batchelor, G. K., "Axial Flow in Trailing Line Vortices," *Journal of Fluid Mechanics*, Vol. 20, No. 4, 1964, pp. 645–58.
[39] Green, S. I., "Introduction to Vorticity," in *Fluid Vortices*, edited by S. I. Green, Kluwer Academic Press, Dordrecht, The Netherlands, 1995, Chap. 10, pp. 427–470.
[40] Donaldson, C duP., Snedeker, R. S., and Sullivan, R. D., "Calculation of the Wakes of Three Transport Aircraft in Holding, Takeoff, and Landing Configurations, and Comparison with Experimental Measurements," Aeronautical Research Associates of Princeton Inc., Report No. 190, 1973, AFSOR TR-73-1594.

P. Givi
Associate Editor